A Series of Strong Earthquakes in Chile at the Beginning of the 21st Century: Similarities, Differences, Relationship

I. S. Vladimirova[1] , Y. V. Gabsatarov[1] , N. S. Shcheveva[1]

[1]Shirshov Institute of Oceanology of Russian Academy of Sciences, Moscow, Russia
* **Correspondence to:** Irina Vladimirova, vladimirova.is@ocean.ru

Abstract: In less than six years, three devastating earthquakes with magnitude exceeding 8.0 have occurred over the Chilean subduction zone. These events were quite well recorded by permanent GNSS stations. We used finite element modeling for a spherically symmetric layered Earth and machine learning methods to investigate the geodynamic processes preceding and accompanying the Chilean earthquake sequence. We find that preseismic coupling before all events is strongly correlated with the coseismic slip distribution, while afterslip primarily located around the coseismic slip patches. We also found that large geologic structures of the oceanic plate have a decisive influence on the development of geodynamic processes in the rupture zones of large Chilean earthquakes.

1. Introduction

The first two decades of the 21st century were marked by an alarming surge in strong earthquakes all over the world. During this period, great earthquakes with magnitudes exceeding 8 occurred in many seismically active regions of the Earth. Three such strong seismic events have occurred over the Chilean subduction zone in less than six years: the 2010 Maule earthquake ($M_W = 8.8$), the 2014 Iquique earthquake ($M_W = 8.1$) and the 2015 Illapel earthquake ($M_W = 8.3$).

All these earthquakes are the shallow-depth megathrust events that ruptured the long-lived seismic gaps. The main objective of our research is to study and compare the deformation processes preceding and accompanying each of the three $M \geq 8$ earthquakes in Chile, and to identify the factors controlling the accumulation and release of stress during strong earthquakes.

2. Data and methods

The dataset used in this study consists of three-component time series from 111 permanent GNSS stations over the 2007–2016 period provided by Nevada Geodetic Laboratory.

We constructed the finite-fault models to investigate the distribution of preseismic coupling along the fault zones as well as the distribution of coseismic slip and afterslip. The geometric design of the finite-fault models was based on the aftershock distribution. To estimate the interplate coupling, coseismic slip and afterslip distribution, we inverted preseismic velocities, coseismic offsets and postseismic displacements using the constrained damped least squares [*Gill et al.*, 1984] over a uniform rectangular grid.

The inversion minimizes the objective function:

$$F = \|w(Gm - d)\|_{L_2}^2 + \lambda \|m\|_{L_2}^2.$$

The first term represents the misfit between modeled Gm and observed velocities/displacements d, and the second term provides a regularization of the solution. Here w is a weight vector inferred from observation uncertainties, G is a matrix consisting of convolutions of the corresponding Green's functions and unit displacements over the subfaults, m is a vector of estimated model parameters and λ is a positive damping factor [*Steblov et al.*, 2023]. We calculated Green's functions for a spherically layered Earth model using a method described in [*Pollitz*, 1996]. To evaluate the capability of the damped least squares method in reconstructing the spatial variation of the slip or coupling distribution, we perform the checkerboard tests as described in [*Steblov et al.*, 2023].

The modeling of postseimic processes is a challenging task since potential candidates for intense postseismic deformation after the megathrust events are afterslip, viscoelastic relaxation and poroelastic rebound. Distinguishing between these different mechanisms is nearly impossible based on only GNSS data. It is believed that vertical postseismic deformations may be an indicator of the dominant postseismic mechanism e.g., [*Nishimura et al.*, 2003]. However, the use of vertical observations is somewhat complicated due to their smaller amplitude compared to horizontal ones and, at the same time, larger observation errors, as well as due to the superposition of tectonic and non-tectonic signals (for example, surface loads) [*Wang et al.*, 2016]. Moreover, according to recent studies, vertical deformation during the seismic cycle shows significant spatiotemporal variations depending on the mechanical properties and fault kinematics [*Li et al.*, 2024]. Therefore, the vertical displacement pattern is difficult to interpret unambiguously.

To shed some light on the on the spatially and temporally dominant postseismic mechanism after the Chilean earthquakes we perform regression analysis of continuous GNSS time-series using machine learning methods. The solution for best regression model parameters was obtained by a minimization of an empirical risk functional $\min_{\theta \in \Theta} \|p(T)\theta - Y\|_{L_2}^2$, where $\theta \in \Theta = \mathbb{R}^M$ is a model parameter vector, $T \in \mathbb{R}$ is a set of time moments, $Y \in \mathbb{R}$ is a set of time series values,

$$p(t) = \begin{array}{l} (1, t, \sin(2\pi t), \cos(2\pi t), \sin(4\pi t), \cos(4\pi t), H(t > T_0), \dots, \\ H(t > T_l), H(t > T_0^{\text{post}}) \cdot \text{post}_0(t), \dots, H(t > T_k^{\text{post}}) \cdot \text{post}_k(t)) \end{array}$$

is a feature vector, H is a Heaviside function, $\text{post}_i(t) = \left(\ln\left(1 + \frac{t}{\tau_a}\right), -\exp\left(-\frac{t}{\tau_b}\right)\right)$ is a postseismic features vector for i-th event [*Sobrero et al.*, 2020], τ is a decay time. Here we neglect the poroelastic rebound due to large distances from the sources to GNSS stations. Moments of earthquakes l and onsets of postseismic processes k (Figure 1) was determined using the Change Point Detection (CPD) approach [*Truong et al.*, 2020].
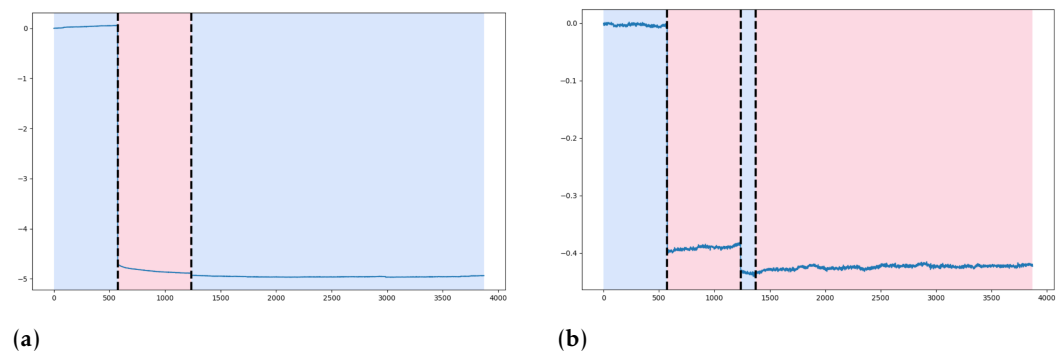

(a)   **(b)**

Figure 1. Results of applying the CPD algorithm to the east (a) and north (b) components of time series of the GNSS-station CONT (Conception, Chile). Dashed lines denote the instantaneous shifts.
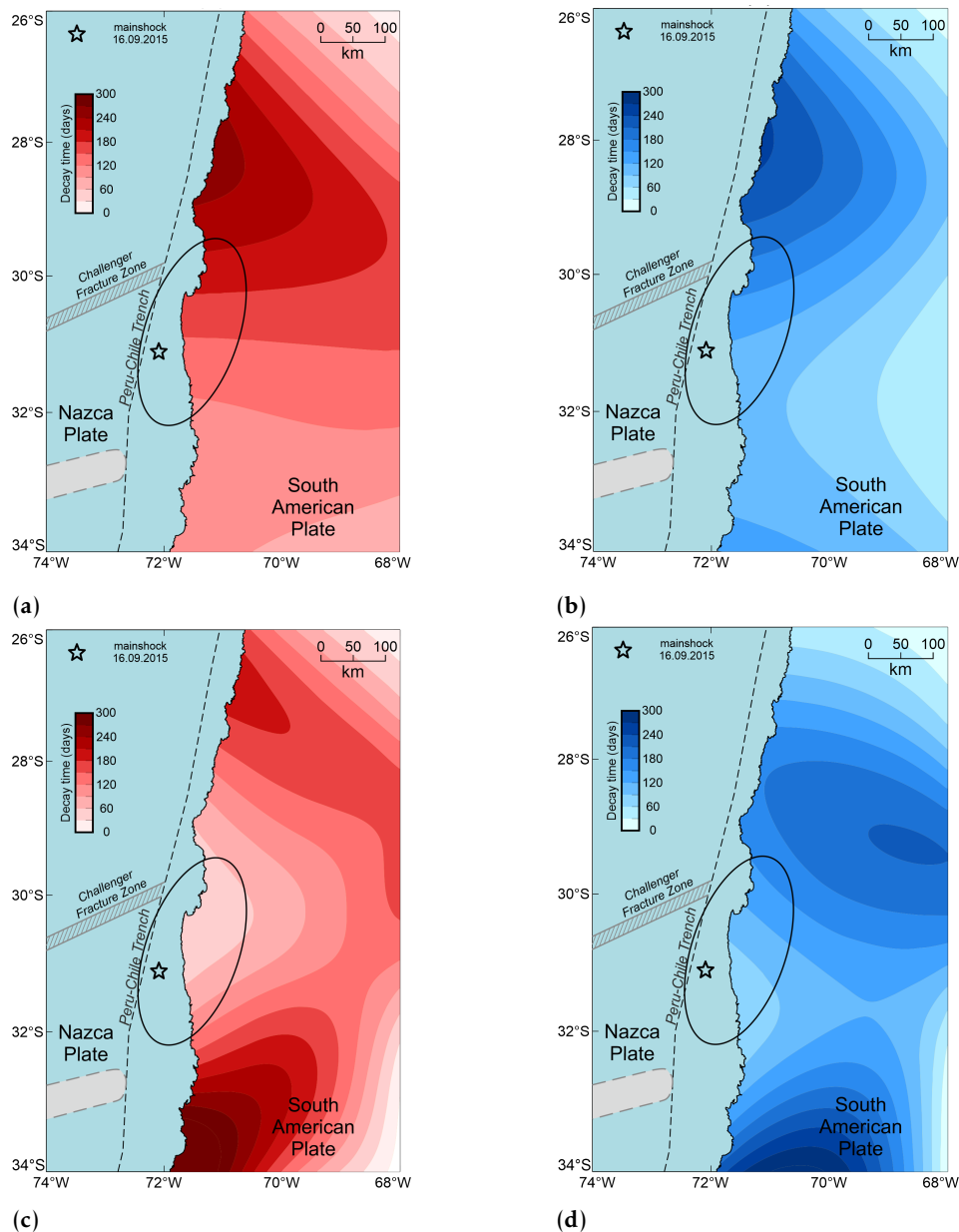
Figure 2. Geographical distribution of logarithmic (a, b) and exponential (c, d) decay times after the 2015 Illapel earthquake. Red and blue colors denote east and north components, respectively.

The estimated decay constants τ_a and τ_b show prominent domination of afterslip in the near-field and viscoelastic relaxation in the far-field towards the continent. An example of estimated decay fields for 2015 Illapel earthquake is shown on Figure 2.

3. Results

Our inverted preseismic coupling, coseismic slip and afterslip distributions for the 2010 Maule, 2014 Iquique and 2015 Illapel earthquakes are represented on Figure 3–5. These models agree in their main characteristics (location of areas of maximum displacements, size of earthquake sources, etc.) with similar models obtained from the inversion of teleseismic body waves (e.g., [*Lay et al.*, 2014; *Pulido et al.*, 2011]), joint inversion of tsunami waveforms and geodetic or teleseismic data (e.g., [*Gusman et al.*, 2015; *Heidarzadeh et al.*, 2016]) as well as joint inversion of GNSS and InSAR data (e.g., [*Klein et al.*, 2017; *Lin et al.*, 2013]).

The results of our modeling show good spatial agreement between location of locked patches (Figure 3a, 4a, 5a) and areas of stress release (Figure 3b, 4b, 5b) for all studied earthquakes.

The afterslip models (Figure 3c, 4c, 5c) show a predominantly dipping and along-strike development of rupture zones, which indicate the postseismic stress release in patches adjacent to areas of high coseismic slip.
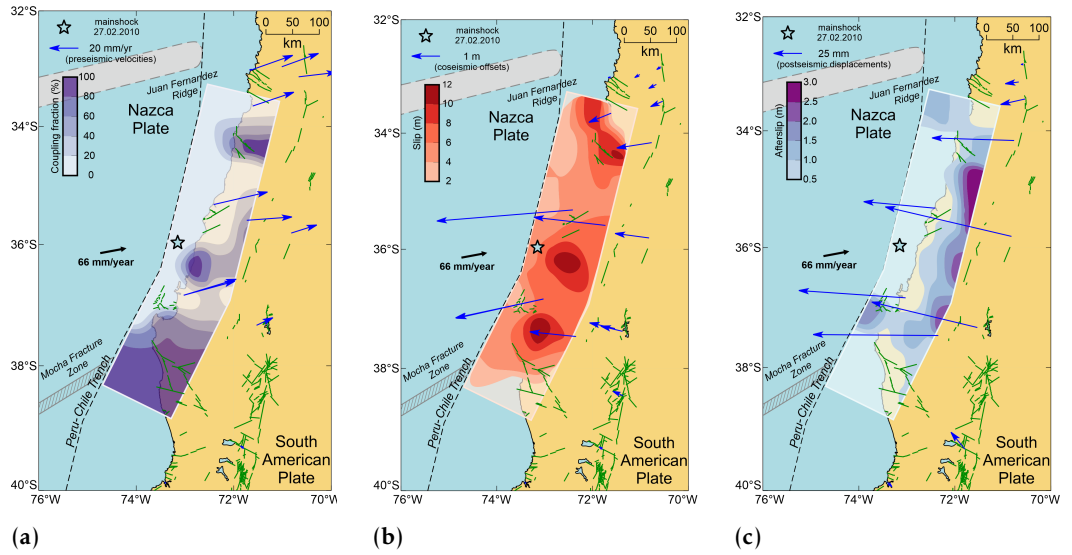

(a)   **(b)**   **(c)**

Figure 3. Models of preseismic coupling (a), coseismic slip (b) and 6-months afterslip (c) in the 2010 Maule rupture zone. The star is the mainshock (gCMT). Blue vectors indicate the GNSS data. Green lines show active regional faults [*Maldonado et al.*, 2021].

(a)   **(b)**   **(c)**
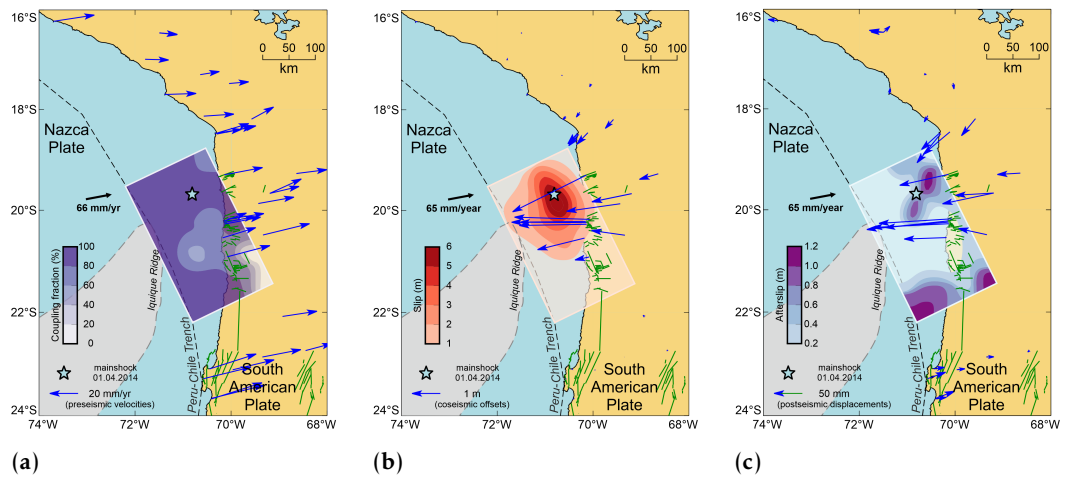
Figure 4. Models of preseismic coupling (a), coseismic slip (b) and 6-months afterslip (c) in the 2014 Iquique rupture zone. Designations according to Figure 3.

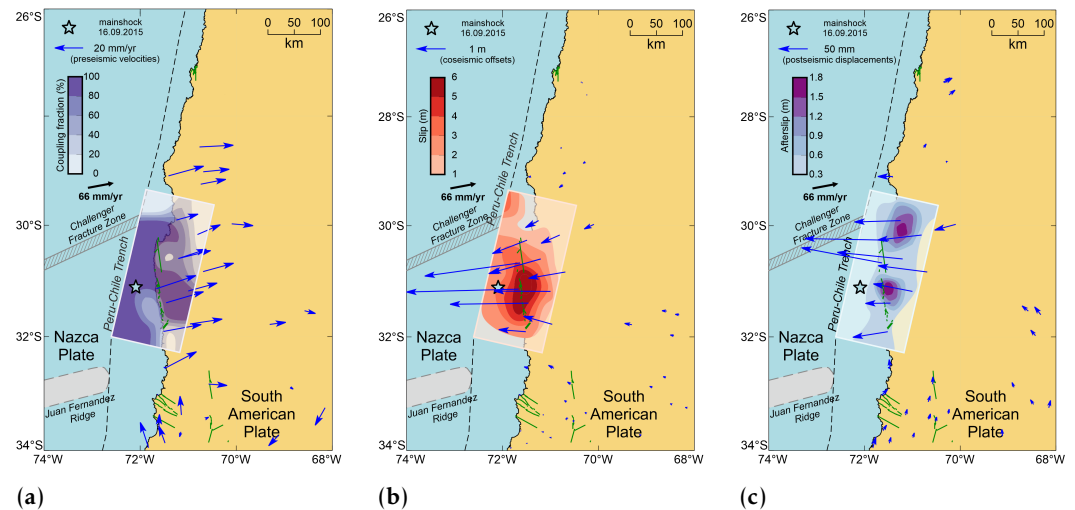**(a)**   **(b)**   **(c)**

Figure 5. Models of preseismic coupling (a), coseismic slip (b) and 6-months afterslip (c) in the 2015 Illapel rupture zone. Designations according to Figure 3.

Comparison of our inverted models and regional morphostructures show that large geological features of the oceanic plate act as natural boundaries of rupture zones, while active tectonic structures of the continental margin have a local influence on the processes of stress accumulation and release.

4. Conclusion

We have modeled the preseismic coupling as well as coseismic slip and afterslip on three megathrust earthquakes rupture zones in Chile based on GNSS data.

We inferred thst postseismic deformations localized around the mainshock rupture zone are most likely explained by afterslip, whereas long-term diffuse deformations observed in the far field can be explained by viscoelastic relaxation of the lower crust or upper mantle.

We also found that large geologic structures of the oceanic plate have a decisive influence on the development of geodynamic processes in the rupture zone.

References

Gill P. E., *Murray W.*, *Saunders M. A.*, *et al.* Procedures for optimization problems with a mixture of bounds and general linear constraints // ACM Transactions on Mathematical Software. — 1984. — Vol. 10, no. 3. — P. 282–298. — DOI: 10.1145/1271.1276.

Gusman A. R., *Murotani S.*, *Satake K.*, *et al.* Fault slip distribution of the 2014 Iquique, Chile, earthquake estimated from ocean-wide tsunami waveforms and GPS data // Geophysical Research Letters. — 2015. — Vol. 42, no. 4. — P. 1053–1060. — DOI: 10.1002/2014gl062604.

Heidarzadeh M., *Murotani S.*, *Satake K.*, *et al.* Source model of the 16 September 2015 Illapel, Chile, Mw 8.4 earthquake based on teleseismic and tsunami data // Geophysical Research Letters. — 2016. — Vol. 43, no. 2. — P. 643–650. — DOI: 10.1002/2015gl067297.

Klein E., *Vigny C.*, *Fleitout L.*, *et al.* A comprehensive analysis of the Illapel 2015 Mw 8.3 earthquake from GPS and InSAR data // Earth and Planetary Science Letters. — 2017. — Vol. 469. — P. 123–134. — DOI: 10.1016/j.epsl.2017.04.010.

Lay T., *Yue H.*, *Brodsky E. E.*, *et al.* The 1 April 2014 Iquique, Chile, Mw 8.1 earthquake rupture sequence: Lay et al.: April 1, 2014 Iquique Mw 8.1 earthquake // Geophysical Research Letters. — 2014. — Vol. 41, no. 11. — P. 3818–3825. — DOI: 10.1002/2014gl060238.

Li S., *Chen L.* Vertical Crustal Deformation Due To Viscoelastic Earthquake Cycles at Subduction Zones: Implications for Nankai and Cascadia // Journal of Geophysical Research: Solid Earth. — 2024. — Vol. 129, no. 8. — DOI: 10.1029/2024jb028817.

Lin Y.-n. N., *Sladen A.*, *Ortega-Culaciati F.*, *et al.* Coseismic and postseismic slip associated with the 2010 Maule Earthquake, Chile: Characterizing the Arauco Peninsula barrier effect // Journal of Geophysical Research: Solid Earth. — 2013. — Vol. 118, no. 6. — P. 3142–3159. — DOI: 10.1002/jgrb.50207.

Maldonado V., *Contreras M.*, *Melnick D.* A comprehensive database of active and potentially-active continental faults in Chile at 1:25,000 scale // Scientific Data. — 2021. — Vol. 8, no. 1. — DOI: 10.1038/s41597-021-00802-4.

Nishimura T., *Thatcher W.* Rheology of the lithosphere inferred from postseismic uplift following the 1959 Hebgen Lake earthquake // Journal of Geophysical Research: Solid Earth. — 2003. — Vol. 108, B8. — DOI: 10.1029/2002jb002191.

Pollitz F. F. Coseismic Deformation From Earthquake Faulting On A Layered Spherical Earth // Geophysical Journal International. — 1996. — Vol. 125, no. 1. — P. 1–14. — DOI: 10.1111/j.1365-246x.1996.tb06530.x.

Pulido N., *Yagi Y.*, *Kumagai H.*, *et al.* Rupture process and coseismic deformations of the 27 February 2010 Maule earthquake, Chile // Earth, Planets and Space. — 2011. — Vol. 63, no. 8. — P. 955–959. — DOI: 10.5047/eps.2011.04.008.

Sobrero F. S., *Bevis M.*, *Gómez D. D.*, *et al.* Logarithmic and exponential transients in GNSS trajectory models as indicators of dominant processes in postseismic deformation // Journal of Geodesy. — 2020. — Vol. 94, no. 9. — DOI: 10.1007/s00190-020-01413-4.

Steblov G., *Vladimirova I.* Geodetic Inversions and Applications in Geodynamics // Applications of Data Assimilation and Inverse Problems in the Earth Sciences. — Cambridge University Press, 2023. — P. 278–292. — DOI: 10.1017/9781009180412.019.

Truong C., *Oudre L.*, *Vayatis N.* Selective review of offline change point detection methods // Signal Processing. — 2020. — Vol. 167. — DOI: 10.1016/j.sigpro.2019.107299.

Wang K., *Tréhu A. M.* Invited review paper: Some outstanding issues in the study of great megathrust earthquakes - The Cascadia example // Journal of Geodynamics. — 2016. — Vol. 98. — P. 1–18. — DOI: 10.1016/j.jog.2016.03.010.